Impact of Promoter Addition on the Regeneration of Ni/Al_2O_3 Dry Reforming Catalysts

Franz, Robert; Pinto, Donato; Uslamin, Evgeny A.; Urakawa, Atsushi; Pidko, Evgeny A.

DOI
10.1002/cctc.202101080

Publication date
2021

Document Version
Final published version

Published in
ChemCatChem

Impact of Promoter Addition on the Regeneration of Ni/Al_2O_3 Dry Reforming Catalysts

Robert Franz,[a] Donato Pinto,[b] Evgeny A. Uslamin,[a, c] Atsushi Urakawa,[b] and Evgeny A. Pidko*[a]

Industrial-scale reforming of methane is typically carried out with an excess of oxidant to suppress coking of the catalyst. On the other hand, many academic studies on dry reforming employ a CO_2/CH_4 ratio of unity to quickly observe coking which can be reduced by adding a catalyst promoter. In this work, Ni/Al_2O_3 catalysts were tested for dry reforming of methane ($CO_2/CH_4 = 1$) with additional regeneration steps to test the resistance against an oxidation treatment. Thereby, we wanted to evaluate catalyst stability for industrial relevance. The effects of three promoters, Cr, Mn and Fe, that differ in their degree of CO_2 interaction, are compared. A higher iron loading on Ni/Al_2O_3 leads to higher stability in dry reforming with lower coke formation. However, the higher the concentration of a promoter with high CO_2 affinity, the quicker the catalyst is oxidized during regeneration with CO_2. Subsequent reduction of a catalyst oxidized with CO_2 leads to considerable sintering in all cases. This sintering induces formation of more coke during dry reforming. On such sintered samples only highly effective promoters in large concentrations still have a noticeable effect compared to unpromoted Ni/Al_2O_3.

1. Introduction

Dry reforming of methane is a reaction that has received a lot of attention in academic and industrial research in the last decades. The growing issue of global warming requires society to find an effective approach to decrease the amount of CO_2 emissions into the atmosphere. One potential approach to achieve a reduction in emissions is to use CO_2 as a chemical resource. Good examples for this approach are reactions such as the hydrogenation of CO_2 to hydrocarbons[1] and methanol[2] or dry reforming of methane (DRM).[3] The latter refers to the combined conversion of methane and CO_2 to synthesis gas or syngas [Eq. (1)]:

$$CH_4 + CO_2 \rightarrow 2CO + 2H_2 \quad \Delta H_{298K} = 247 \text{ kJ mol}^{-1} \tag{1}$$

This reaction has several important advantages. Firstly, not only CO_2 is used, but also methane, which is also a highly active greenhouse gas.[4] Secondly, synthesis gas is an intermediate for many large-scale chemical reactions and widely synthesized via steam reforming of hydrocarbons [Eqs. (2)-(3)]:

$$CH_4 + H_2O \rightarrow CO + 3H_2 \quad \Delta H_{298K} = 206 \text{ kJ mol}^{-1} \tag{2}$$

$$C_mH_n + m\ H_2O \rightarrow m\ CO + \left(m + {}^{n}/_{2}\right) H_2 \tag{3}$$

DRM therefore represents an attractive CO_2 utilization route that can draw on a vast amount of expertise and infrastructure already available within the chemical industry. In contrast to steam reforming of methane (SRM) the additional energy input for water evaporation is not necessary for DRM.[3c] Nevertheless, this reaction is only slowly being implemented in industry. The feed in DRM is more carbon rich than in SRM, leading to a higher propensity to coke formation and catalyst deactivation.[3c,5] The DRYREF process developed by BASF and Linde is less harsh than pure dry reforming since both steam and CO_2 are used as the oxidant. Even so, existing steam reforming catalysts were not sufficiently resistant to coke formation under these conditions, requiring an extensive period of catalyst optimization.[6]

Commercial steam reforming catalysts are mostly based on nickel as the active component since it offers an acceptable compromise between activity, stability, cost and availability.[3c,7] To prevent excessive coke formation, different strategies have been reported in literature. The most common approach in catalyst design is to add another metal to the catalyst as a promoter. These metals can improve the performance in several different manners. It has been shown that coke is mainly formed on larger Ni particles or on step-edge sites on the Ni surface.[3b,8] Promotors block such highly reactive sites and thus

[a] Dr. R. Franz, Dr. E. A. Uslamin, Prof. E. A. Pidko
Inorganic Systems Engineering Group
Chemical Engineering Department
Delft University of Technology
Van der Maasweg 9, 2629 HZ Delft (The Netherlands)
E-mail: e.a.pidko@tudelft.nl
[b] D. Pinto, Prof. A. Urakawa
Catalysis Engineering
Chemical Engineering Department
Delft University of Technology
Van der Maasweg 9, 2629 HZ Delft (The Netherlands)
[c] Dr. E. A. Uslamin
TsyfroCatLab Group
University of Tyumen
Volodarskogo St.6, 625003, Tyumen (Russia)

Supporting information for this article is available on the WWW under https://doi.org/10.1002/cctc.202101080

suppress coke formation. Most popular promotors of this type are alkali and earth alkali metals.[9] A similar mode of action has also been reported for other common metal promotors such as Mn or Sn.[10]

Besides the site-blocking, promoters can introduce other beneficial effects. Alkali metals can enhance CO_2 adsorption via a carbonate cycle.[9b,11] Mn, Sn and several noble metals stabilize small Ni particles.[10a,12] Additionally, Mn has also been reported to increase the CO_2 affinity of the catalyst.[10c] A control over the particle size can also be achieved via the selection of catalyst support materials.[13] Lastly, promoters can bring about enhanced redox reactivity to help coke removal through a redox cycle of the promoter, i.e. via a Mars-van Krevelen mechanism. The prime example for such an effect is the addition of Fe to a Ni-based catalyst, which allows either for a chemical looping process or continuous operation with little coke deposition.[14]

Despite decades of research, catalyst deactivation due to coking is a persistent problem in DRM. This makes cyclic operation, in which the catalyst is periodically regenerated, an attractive strategy to manage carbon formation. Various procedures utilizing different regeneration gases and conditions are available.[15] Coke can be removed from the catalyst surface either by oxidation with CO_2 or O_2 or by methanation with H_2. Oxidative regeneration is preferable in an industrial setting as it does not affect the overall yield of the target product H_2. A common drawback of this approach is the considerable sintering of the metal particles due to oxidation.[15a,16] *Takenaka et al.* investigated the influence of the support on Ni stability in cycles of methane decomposition and coke gasification with CO_2.[15d] Ni/SiO_2 was found to be the most prone to sintering. The increase of particle sizes due to the cyclic operation occurred to a lesser extent for Ni/TiO_2 and Ni/Al_2O_3. *Düdder et al.* demonstrated that CO_2 regeneration allows for the full recovery of the initial activity of a $Ni/MgAlO_X$ catalyst.[15b] However, no information on the effect of the regeneration on the Ni particles was presented.

In-situ XAS studies by *Steib et al.* demonstrated that a catalyst regeneration with CO_2 at 800 °C oxidizes the Ni phase on various supports.[15c,17] Exposure of Ni/SiO_2 and Ni/ZrO_2 to the original reaction mixture of CH_4 and CO_2 is sufficient to reduce the Ni again. In contrast, more Ni is in the oxidized state in the second reaction cycle than in the first cycle for Ni/Al_2O_3.

This information on Ni oxidation during catalyst regeneration raises the question of what the impact of promoter addition is on catalyst stability during regeneration. The mechanisms, by which promoters increase catalyst stability, include differing degrees of interaction with CO_2. Therefore, in this work we compare the effect of promoters that vary in their degree of interaction with CO_2 on the stability of Ni/Al_2O_3 catalysts. Literature led us to Cr, Mn and Fe as representative promoters since they present an increasing level of interaction with CO_2. Cr is not reported to noticeably increase the interaction of Ni-catalysts with CO_2, while Mn enhances the CO_2 adsorption on Ni/Al_2O_3 catalysts and Fe is redox active.[10b,c, 14c, d] Our results show that the more the promoter interacts with CO_2 the more the catalyst is deactivated during a regeneration procedure consisting of a short exposure to a stream of diluted CO_2. We assume this deactivation to be due to catalyst oxidation. An additional reduction of a thus fully oxidized catalyst causes a significant increase in coke formation during dry reforming compared to a fresh catalyst. Only high loadings of effective promoters limit this increase in coking after regeneration to a reasonable degree.

It must also be mentioned that commercial methane reforming is typically carried out with an excess of oxidant to suppress coke formation.[3b] The ensuing concentration gradient over the length of the catalyst bed results in an oxidizing atmosphere in the upper section of the catalyst bed where little methane conversion has taken place.[18] Thus, catalyst stability under oxidative environments is a relevant parameter in general. The research in this work presents model experimental investigations of this stability making the conclusions relevant beyond the immediate application of catalyst regeneration.

Experimental

Chemicals

The following chemicals were used in this work: Ethylenediaminetetraacetic acid (EDTA, ThermoFisher 99%), NH_3 solution (VWR, 25 wt.%), γ-Al_2O_3 catalyst support (Alfa Aesar), $Ni(NO_3)_2 \cdot 6H_2O$ (Merck, analysis quality), $Mn(NO_3)_2 \cdot 4H_2O$ (Acros, analysis quality), $Cr(NO_3)_3 \cdot 9H_2O$ (Sigma Aldrich, 99%), $Fe(NO_3)_3 \cdot 9H_2O$ (Sigma Aldrich 98%).

All materials were used as received except for NH_3 (aq.) and Al_2O_3. NH_3 (aq.) was diluted with demineralized water to achieve concentrations of 12 wt.% and 5 wt.%. Al_2O_3 extrudates were ground to a particle size below 212 μm and calcined at 800 °C for 4 h (10 °C min^{-1} heating rate) before impregnation.

Catalyst preparation

All samples were synthesized via sequential incipient wetness impregnation. EDTA is used as a chelating agent to achieve a more uniform distribution of the metals and a higher dispersion. The approach is based on available literature on this topic.[19] In a typical synthesis EDTA and $Ni(NO_3)_2$ or the nitrate salt containing the promoter were dissolved in an aqueous ammonia solution and impregnated on the support. After each impregnation, the sample was dried at 80 °C for 6 h and then calcined at 700 °C for 5 h (10 °C min^{-1} heating rate). The solubility of the different nitrates and EDTA together in the aqueous ammonia solution varied. The amount of EDTA also had to be varied depending on the promoter to achieve reproducibility of the catalytic tests. For Ni, 12 wt.% NH_3 and a Ni/EDTA molar ratio of unity were used. The promoter was always impregnated before the nickel and in some cases over multiple impregnation steps. The catalysts with promoter are named according to the system y.yyX1Ni, in which y.yy is the molar ratio of the promoter X (Cr, Mn or Fe) to Ni. The final, optimized values are given in Table 1.

Catalyst characterization

Temperature programmed reduction (TPR) was carried out in a home-built setup equipped with thermal conductivity detector (TCD) and mass spectrometer (MS). For TPR measurements, 100 mg of sample (particle size 212–355 μm) were filled into a quartz reactor (I.D. of 6 mm) and the reactor placed into the furnace.

Table 1. Overview of the synthesis parameters.

Sample name	Ni loading [g $g_{support}^{-1}$]	$n(M^{n+})/n(Ni^{2+})$	$n(EDTA)/n(M^{n+})$	c(NH_3) [wt.%]
REF	0.08	0	–	12
1Mn1Ni	0.08	1	2	12
0.5Mn1Ni	0.08	0.5	2	12
0.25Mn1Ni	0.08	0.25	2	12
1Cr1Ni	0.08	1	3	12
0.5Cr1Ni	0.08	0.5	3	12
0.25Cr1Ni	0.08	0.25	3	12
1Fe1Ni	0.08	1	1	5
0.5Fe1Ni	0.08	0.5	1	5
0.25Fe1Ni	0.08	0.25	1	5

Afterwards, a flow of 30 mL min^{-1} (10% H_2 in Ar) was started. The setup was heated to 950 °C with a ramp of 10 °C min^{-1}. H_2 consumption was monitored with the TCD downstream of the reactor.

CO_2 Temperature-programmed desorption (CO_2-TPD) was measured in the same setup as the TPR experiments. For each measurement 150 mg of sample (particle size 212–355 μm) were filled into a quartz reactor (I.D. of 6 mm) and the reactor placed into the furnace. In a first step, the sample was reduced using a flow of 30 mL min^{-1} at 800 °C for 1 h (heating rate of 10 °C min^{-1}). Then the sample was cooled in 27 mL min^{-1} of pure Ar to room temperature. After cooling, the sample was exposed to 25 mL min^{-1} of CO_2 for 30 minutes. The flow was then switched again to 27 mL min^{-1} of Ar and the system was purged until the CO_2 signal in a mass spectrometer downstream of the reactor was stable. Once the baseline was stable, the furnace temperature was increased to 800 °C with a rate of 10 °C min^{-1}.

NH_3-TPD was measured using a *Micromeritics Autochem II 2920* unit. For each measurement 200 mg of sample were loaded into the system and heated under H_2 flow to 800 °C (10 °C min^{-1}). After 1 h of reduction at this temperature the sample was cooled to a temperature of 200 °C under He flow. Once the sample was stabilized at this temperature the flow was switched to 3% NH_3 in He and maintained for 1 h. Finally, after the exposure to NH_3, the flow was switched to He again and the sample was heated to 750 °C with a rate of 10 °C min^{-1}.

H_2-Chemisorption measurements were performed in a *Micromeritics ASAP 2020 C*. 400 mg of sample per measurement were loaded into the sample tube. The system was heated to 800 °C under H_2 flow (5 °C min^{-1}) and this temperature maintained for 1 h. The sample was then cooled to 35 °C and the H_2 uptake was measured. This was followed by two more measurement cycles for each sample. In the second cycle the samples were heated to 700 °C (5 °C min^{-1}) and exposed first to CO_2 for 30 min and then to H_2 for 30 minutes before cooling to measurement temperature. For the third cycle the original reduction procedure at 800 °C was used. To account for H_2 physisorption, all reported values are the difference in uptake between two consecutive H_2 chemisorption measurements with an evacuation step in between.

TEM images were obtained using a Jem JEOL 1400 transmission electron microscope. The equipment was operated at 120 kV using a single-tilt holder. Calcined catalysts were ground to a fine powder and dispersed in denatured ethanol. This dispersion was dropped onto Quantifoil R 1.2/1.3 holey carbon films supported on a Cu mesh.

XRD analyses were carried out with a Bruker D8 Advance Diffractometer using monochromatic Co Kα radiation (λ = 0.179026 nm) at room temperature.

N_2 physisorption was carried out after drying all samples overnight at 150 °C under a flow of N_2. The samples were then loaded into a *micromeritics TriStar II*. The measurements were done at 77 K.

Catalytic testing

The catalytic tests for dry reforming of methane were carried out in a single-reactor system. The reactor consists of a quartz tube (I.D. of 4 mm) in a furnace. Bronkhorst mass flow controllers upstream of the reactor control the flow of N_2, CH_4, CO_2 and H_2. Downstream of the reactor a compact GC equipped with a TCD was used for the online product analysis. Product separation was achieved using a micropacked column (ShinCarbon ST 80/100 2 m, 0.53 mm I.D.). The conversion of methane and CO_2 was calculated using N_2 as the internal standard according to Equation (4):

$$X_R = \frac{\left(A_R/A_{N2}\right)_0 - \left(A_R/A_{N2}\right)}{\left(A_R/A_{N2}\right)_0} \quad (4)$$

where R is the reactant in question (either CH_4 or CO_2) and A is the peak area in the GC. In all experiments, 10 mg of sample (355–425 μm) were diluted in 140 mg of SiC (212–300 μm). This mixture was filled into the quartz reactor between two plugs of quartz wool and upstream of a 9 cm layer of SiC (212–425 μm). To pre-warm the feed a 7 cm bed of SiC (212–425 μm) was placed upstream of the catalytic bed. In all experiments the fresh sample was heated in a stream of 10% H_2 in N_2 (50 mL min^{-1}) to 800 °C (10 °C min^{-1}) and reduced at this temperature for 1 h, before being cooled to 650 °C. Afterwards, the flow was switched to 100 mL min^{-1} of 25% CH_4 and 25% CO_2 in N_2. Standard activity measurements consisted of 24 h of reaction. The sample was then either cooled down to room temperature or heated to 700 °C for a regeneration treatment. One treatment consisted of 30 min of CO_2 exposure (50 mL min^{-1} of 40% CO_2 in N_2) followed by 30 min of reduction (50 mL min^{-1} of 10% H_2 in N_2). The other regeneration protocol was an exposure to CO_2 of 4 min (50 mL min^{-1} of 40% CO_2 in N_2). In all cases heating and cooling before and after the regeneration treatment were done under pure N_2 flow. A second reaction cycle of 24 h at 650 °C was added after the regeneration procedure if desired. Lastly, the entire system was cooled to room temperature under N_2 flow. After each catalytic experiment, the coke content of the sample was analyzed by TGA (Mettler-Toledo TGA/SDTA 851[e]). For the activity measurements in standard dry reforming two different batches of catalyst were tested to determine the experimental error in both coke content and conversion.

The experiments to visually check for signs of catalyst oxidation under elevated CO_2 concentrations were carried out in two different setups. In one case 50 mg of undiluted catalyst (212–425 μm) were loaded into the setup described above and with the same amounts of SiC upstream and downstream of the catalyst bed. The catalyst was then reduced in 10% H_2 in N_2 (50 mL min^{-1}) at 800 °C for 1 h (10 °C min^{-1}). The reactor was afterwards cooled to 650 °C and the flow switched to 12.5% CH_4 and 25% CO_2 in N_2 (100 mL min^{-1}) and the reaction was carried out for 30 h.

Operando monitoring of the CO_2 regeneration was carried out in a different setup. It consists of a single quartz tube reactor (4 mm I.D.) in a furnace with Bronkhorst mass flow controllers upstream. In this setup the quartz reactor is equipped with a steel jacket to ensure a homogeneous heat transfer to the catalyst bed. This steel jacket contains an opening to allow for observation of the catalyst bed. Similarly, the wall of the furnace contains a glass window above of which a digital microscope was positioned to take pictures of the catalyst bed during reaction. In total 50 mg of catalyst (212–

425 μm) were placed in the reactor, heated to 800 °C in a flow of 50 mL min^{-1} of H_2 (10 °C min^{-1}) and reduced at this temperature for 1 h. Afterwards the system was cooled to 650 °C and the sample exposed to 40 mL min^{-1} of 10% CO_2 in He. During this time, the change in sample color was monitored with the digital microscope. Simultaneously, the outlet gas mixture was analyzed with a high temporal resolution (5 s per spectrum) by means of an ALPHA FTIR spectrometer (Bruker). The obtained interferograms were then Fourier-transformed and the absorbance area was evaluated in the spectral ranges of 2260–2280 cm^{-1} and 2040–2060 cm^{-1} and used for CO_2 and CO quantification respectively. Calibration of this system was carried out with gas mixtures of known composition. The degree of catalyst oxidation was calculated from the generated CO and the desired catalyst loading, using Equation (5):

$$D_O(t) = \frac{n_{CO}(t)}{n_{Ni} + 1.5^{*} n_{Fe}} \times 100 \quad (5)$$

in which $D_O(t)$ is the degree of oxidation at time t in %, $n_{CO}(t)$ the total molar amount of CO released until that time and n_{Ni} and n_{Fe} the molar amounts of Ni and Fe on the used sample. The factor of 1.5 stems from the assumption that Fe(0) is oxidized to Fe_2O_3. Ni(0) is assumed to be oxidized to NiO. The obtained pictures of the catalyst bed were processed with Adobe Photoshop 2018 (brightness and contrast) to highlight color changes in the catalyst bed.

2. Results and Discussion

2.1. Catalyst characterization

Temperature-programmed reduction was carried out in a first step to obtain information on the reducibility of the promoted catalysts. The results in Figure 1 show that two peaks were detected for all samples containing the promoters Cr, Mn or Fe. The reduction at lower temperature takes place at 300–500 °C, depending on the sample, with a lower reduction temperature for the Cr-series. The second reduction occurs at 800-900 °C. For REF only a high-temperature reduction was detected and the intensity of the low-temperature peak increases with promoter loading. This clearly assigns the high-temperature reduction to Ni and the low-temperature reduction to the promoter. Especially for the Cr-containing samples the intensity of the promoter peak is more prominent in contrast to the other samples for which significantly less H_2 consumption could be measured.

Cr–Ni catalysts are known to form alloys upon reduction, making Cr(0) the probable final oxidation state.[20] At the same time, oxidized Cr can theoretically be present in different oxidation states up to Cr(VI). Considering the larger peak for Cr reduction compared to the other promoters, we assume that Cr is at least partially present in higher oxidation states than Cr(III). The changes in the Fe-series can at most be from Fe(III) to Fe(0) and these samples contain a significantly smaller promoter reduction peak.[14d] Reduction of supported Mn systems should lead to a maximum change in oxidation state from Mn(IV) to Mn(II).[21]

The promoters were added to the catalyst to increase the interaction of the catalyst with CO_2. To compare the influence of the different promoters on this parameter, temperature-programmed desorption of CO_2 (CO_2-TPD) was measured for the reference sample and all samples with a promoter/Ni ratio of unity. The resulting CO_2-signals shown in Figure 2 highlight that only the addition of manganese leads to a greater adsorption of CO_2 on the catalyst. Chromium and iron do not affect the CO_2 adsorption capacity to any significant degree. The total peak area is comparable for these two samples and the reference Ni/Al_2O_3. Therefore, when comparing the Cr-series and the Mn-series, an increase in CO_2 adsorption must be considered. For Fe-promoted Ni systems literature data show that at reaction conditions Fe increases the interaction via a

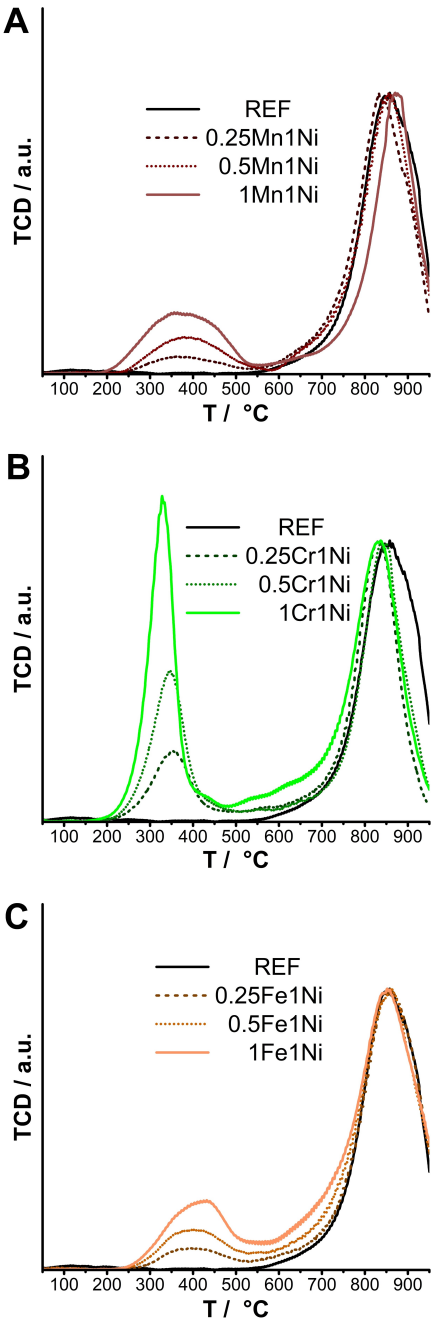

Figure 1. Temperature-programmed reduction of the as-prepared promoted Ni/Al_2O_3 samples: Mn-series (A), Cr-series (B) and Fe-series (C).

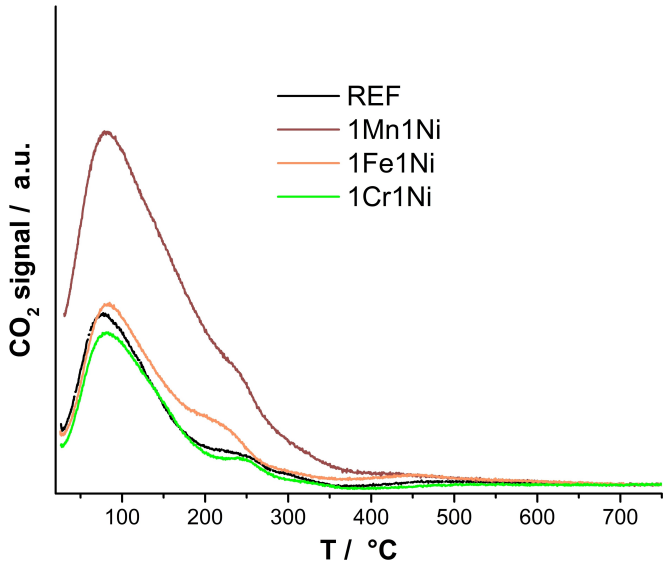

Figure 2. CO_2-TPD profiles for pure Ni/Al_2O_3 and all samples with a promoter/Ni ratio of unity.

redox cycle, which represents a noticeable increase of the interaction with CO_2.[14b,d]

In addition, the catalysts were characterized with H_2 chemisorption. The promoter-Ni interactions can be evaluated by measuring the total metal surface area. Additionally, the regeneration procedures can be simulated in the setup and the impact on the metal surface area compared among the different promoters. The results are summarized in Figure 3. For each series of catalysts only the sample with the highest promoter loading was tested to determine trends. While the samples REF, 1Cr1Ni and 1Fe1Ni have a total metal surface area of approx. 2.5 $m^2 g^{-1}$ after the first reduction at 800 °C, only 1.5 $m^2 g^{-1}$ could be measured for 1Mn1Ni. It is important to note that H_2 chemisorption is not selective for specific metals. Consequently, the simultaneous uptake of H_2 on different metals must be considered. Mn is expected to remain in the oxidic state after reduction[10b], while alloy formation has been reported for Cr–Ni and Fe–Ni systems.[14b,d, 15a, 20] Thus, Mn may block a significant portion of the Ni surface while for the other promoters the total metal surface area remains constant.

Furthermore, the chemisorption setup was used to treat the samples consecutively with CO_2 and H_2 at 700 °C in a similar fashion to the redox regeneration procedure in catalytic testing. Figure 3 also demonstrates how the total metal surface area is affected by a simulated regeneration procedure. In all cases, exposing the catalyst to CO_2 flow and then H_2 flow for 30 min at 700 °C leads to a drop in total metal surface area. This drop is in the range of 10–20% of the original surface area for REF (2.5 to 2.2 $m^2 g^{-11}$) and 1Mn1Ni (1.5 to 1.3 $m^2 g^{-1}$). For 1Cr1Ni this decrease is almost 30% (2.7 to 2 $m^2 g^{-11}$) and for 1Fe1Ni almost no metal surface area could be measured after the redox treatment. A subsequent reduction in H_2 at 800 °C did not drastically change the surface area except for 1Fe1Ni. Approximately 60% of the original surface area was recovered for this sample (2.5 to 1.6 $m^2 g^{-1}$).

Previous studies have shown that exposing Ni catalysts to (diluted) CO_2 at elevated temperatures leads to NiO formation. Especially for Ni/Al_2O_3 the subsequent reduction can be unsuccessful at relatively low temperatures.[15c,d,17] For all tested samples except 1Fe1Ni the surface area increased only marginally after the additional reduction at 800 °C, which suggests that the observed surface area loss is not due to insufficient reduction. Sintering of the Al_2O_3-supported metal particles is the most credible explanation for the loss in surface area measured for REF, 1Mn1Ni and 1Cr1Ni. The reduction behavior of the Fe–Ni system is significantly more complex making it

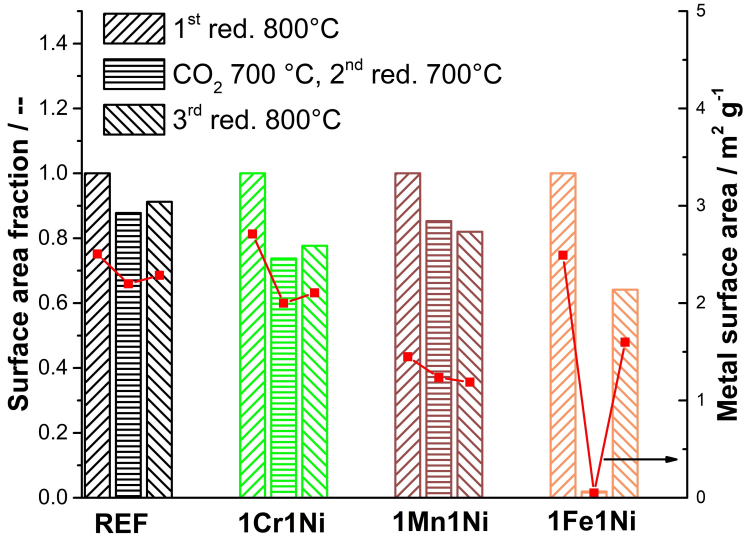

Figure 3. Fraction of metal surface area (columns), determined by H_2 chemisorption, available after CO_2 and/or reduction treatments relative to after the first reduction treatment. The absolute surface area values are shown with closed symbols.

challenging to determine the degree of sintering. For further details we refer to Figure S1.

The catalyst support consists of γ-Al_2O_3 which, while providing a high surface area, contains a non-negligible amount of acid sites. NH_3-TPD was measured for the same samples that were characterized via H_2 chemisorption and CO_2-TPD to judge if the promoters influence the acidity (Figure S2). The addition of Mn appears to reduce the NH_3 uptake slightly which may be related to the higher affinity of CO_2 for 1Mn1Ni. An improved CO_2 uptake has previously been linked to higher catalyst basicity.[10c,22] For 1Fe1Ni NH_3 desorbs at slightly higher temperatures, indicating stronger acidity. Nevertheless, the NH_3 uptake appears to be in a similar order of magnitude for all catalysts.

2.2. Dry reforming of methane

The catalytic tests were carried out at 650 °C which represents a thermodynamic compromise between reforming and coking, allowing for a better insight into the effects of coke formation and the resulting catalyst deactivation.[9b] In a first step, the fresh catalysts were tested for dry reforming of methane without catalyst regeneration. In Figure 4 the methane conversion is plotted for the Mn-series and the Cr-series of catalysts. The coke contents determined after reaction are shown in Figure 5. The respective data for the Fe-series are summarized in Figure 6.

Dry reforming of methane over fresh Ni/Al_2O_3 (REF) shows an initial methane conversion of approx. 40%. Within the first 6–8 h time on stream (TOS) a noticeable deactivation can be observed leading to a conversion of ca. 25%. In the next 16–18 h the deactivation slows down with a final conversion slightly higher than 20% after a total 24 h TOS. Compared to this, the addition of Mn or Cr has a qualitatively similar effect on the conversion. At higher loadings of the promoters the stability of the conversion is increased with a greater effect observed upon the addition of Mn. We attribute the more stable conversion observed for 1Mn1Ni and 0.5Mn1Ni to the higher CO_2 affinity of Mn-promoted catalysts. The experimental variation in conversion between different batches of the same catalyst appears to be greater for 1Mn1Ni and 0.5Mn1Ni than for the corresponding Cr-promoted samples (Figures S3 and S4). Nevertheless, the higher activity for Mn-containing samples in Figure 4 appears to be a valid trend.

The comparison of the coke contents after reaction shown in Figure 5 reveals a similar trend for both Mn and Cr. The coke content is the lowest for the highest promoter loading and the samples 0.5X1Ni (X: Mn or Cr) contain the most coke in both series. The samples 0.25X1Ni only contain slightly less coke than the respective 0.5X1Ni. Interestingly, while for the Cr-series all promoted samples have a lower coke content than the reference sample, both 0.5Mn1Ni and 0.25Mn1Ni contain more coke than the reference Ni/Al_2O_3.

In contrast, the addition of Fe to Ni/Al_2O_3 leads to quite different trends as shown in Figure 6. Especially 1Fe1Ni and 0.5Fe1Ni display an induction period and deactivate much less than the catalyst REF. 0.25Fe1Ni is mainly characterized by its

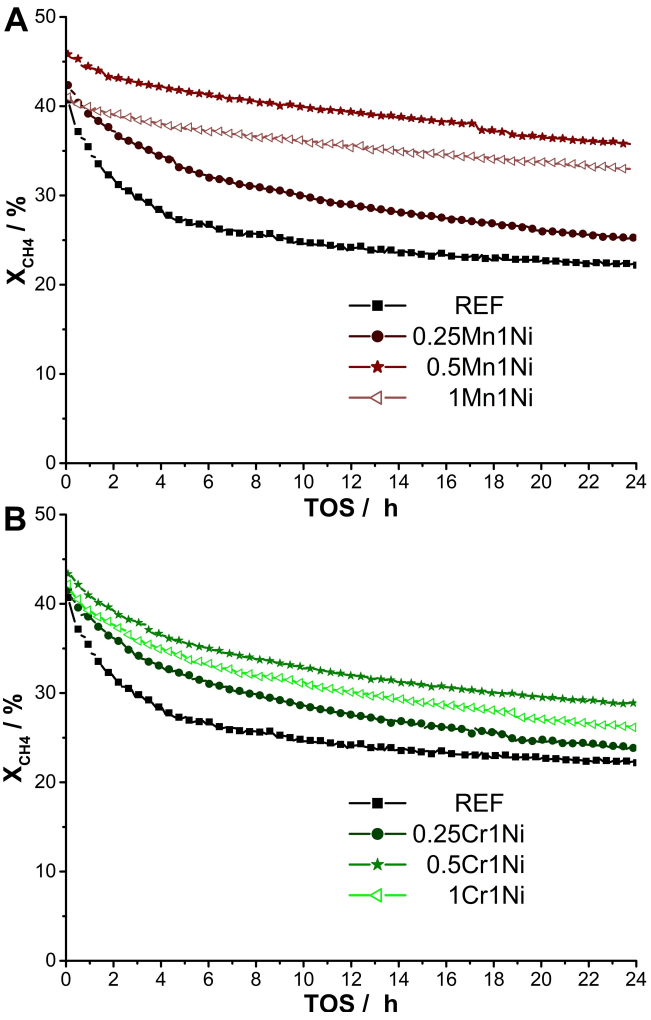

Figure 4. Methane conversion over TOS for Mn (A) and Cr-promoted (B) Ni/Al_2O_3 (10 mg sample, 650 °C, 100 mL min^{-1} of 25% CH_4, 25% CO_2 in N_2).

slow but pronounced deactivation compared to the other Fe-containing samples. With increased Fe-loading, both the induction period and the stabilization of the conversion with TOS become more pronounced. In the case of 0.5Fe1Ni, the conversion first increases to ca. 42% in the first 60 min TOS, after which it decreases very slowly and reaches 40% after 24 h TOS. For the 1Fe1Ni catalyst the induction period is longer, and it takes ca. 2 h TOS to reach a stable conversion of only 30% that remains unchanged during the subsequent 22 h. After the reaction 1Fe1Ni contains 2.4 wt.% coke, which is even less than half the amount formed over pure γ-Al_2O_3. Decreasing the Fe loading leads to increases in the coke content with 13.2 wt.% for 0.5Fe1Ni. To our surprise, a coke content of 33.2 wt.% was measured for 0.25Fe1Ni, which is more than 1.5 times the coke content of REF.

The low coke content for the catalysts with a high Fe-loading can be explained by the Mars-van Krevelen mechanism previously established for Fe–Ni samples, in which surface Fe species actively oxidize coke by participating in a redox cycle.[14b,d] This also explains the lower coke content for 1Fe1Ni

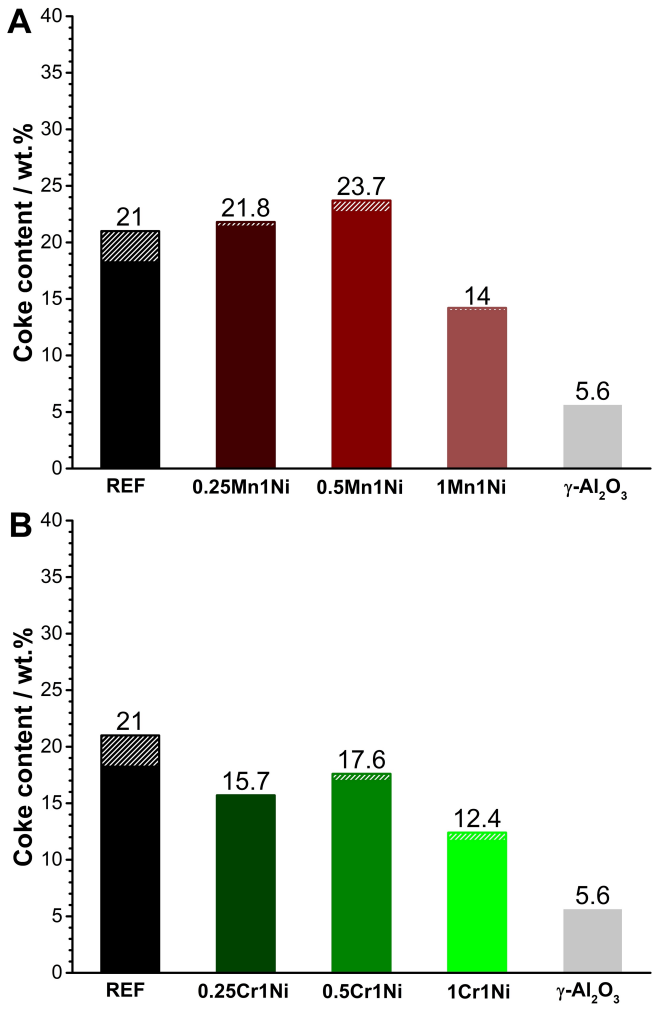

Figure 5. Coke contents as determined by TGA for the Mn-series (A) and Cr-series (B) after 24 h TOS; shaded areas show the observed variation between two measurements (10 mg sample, 650 °C, 100 mL min^{-1} of 25 % CH_4, 25 % CO_2 in N_2).

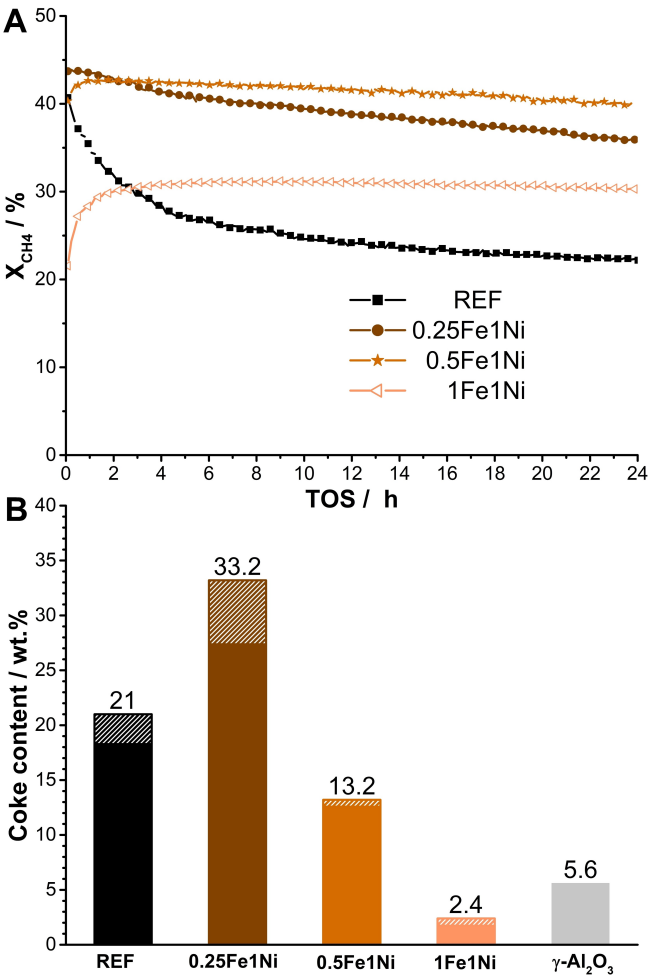

Figure 6. Conversion (A) and coke content after reaction (B) for the Fe-series of Ni/Al_2O_3 catalysts; shaded areas in coke content show the observed variation between different batches (10 mg sample, 650 °C, 100 mL min^{-1} of 25 % CH_4, 25 % CO_2 in N_2).

compared to the pure support. The excessive amount of iron on the catalyst is in contact with carbon deposits forming on the support, oxidizing them as well. At the same time, an Fe-Ni alloy with a high Fe content is less active towards methane than pure Ni or an alloy with a low Fe content.[23] This explains the lower conversion values for 1Fe1Ni despite the improved stability. The negative effect of higher Fe contents in the alloy also partially explains the observed induction periods for 1Fe1Ni and 0.5Fe1Ni. In this context, it is important to mention that the Mars-van Krevelen mechanism leads to partial dealloying and the formation of FeO_X on the surface of the Ni–Fe particles.[14b,d, 23a] Thus, we speculate that in the initial phase of the reaction the reactive metal surface becomes richer in Ni and more active towards methane with small clusters of Fe forming on top of the Fe–Ni particles.

The explanation for the higher coke contents for lower iron loadings is less straightforward. The experimental variation in coke content between different batches is larger for 0.25Fe1Ni than for the other samples. This suggests that the relative distribution of Fe and Ni and thus the degree of interaction between the two metals could at least be partially responsible. Previous studies showed that Ni–Fe systems with low Fe concentrations perform better when synthesized via hydrotalcite-like precursors[14b] than through incipient-wetness impregnation.[14d] The synthesis route via such precursors improves the interaction between Ni and Fe, resulting in a higher catalyst stability.[23a,24] It has been proposed that Fe can increase the lifetime of Ni catalysts for methane decomposition due to the faster diffusion of C through bulk Fe than through bulk Ni.[23a] The presence of Fe in an Fe–Ni alloy thus promotes the diffusion of carbon away from the surface region where methane decomposition takes place, preventing this active site to be blocked by carbon deposits. This implies that a small amount of Fe in the alloy prevents deactivation of the most coke-forming sites which increases the overall amount of coke formed during the reaction. Higher Fe loadings result in a sufficient surface coverage with FeO_X to ensure a noticeable amount of coke removal via the Mars-van Krevelen mechanism.

Over 60 h TOS 1Fe1Ni also starts to show signs of deactivation but less so than REF, 1Mn1Ni and 1Cr1Ni (Figure S5). Only for 1Mn1Ni noticeable additional coke formation could be detected over the extended reaction period. Due to the small amounts of catalyst and the high dilution ratio, we were able to carry out these longer runs without any issues with reactor blocking observed by other researchers.[10b,c] These results confirm that catalytic tests lasting 24 h are sufficient for the analysis of the effects of the regeneration procedures on the catalysts.

Previous studies reported the formation of NiO in supported Ni catalysts upon exposure to CO_2 at high temperatures.[15c,17] To define the regeneration procedures, we investigated the effect of the duration of the CO_2 treatment at 700 °C on the reference catalyst after 24 h of reaction (Figure 7). Interestingly, successful regeneration can only be achieved with short exposures to CO_2. The obvious risk of Ni oxidation led to the investigation of the effects of catalyst oxidation with CO_2, followed by reduction in H_2. For this procedure, a higher activity of the catalyst can be seen in the second reaction cycle. In literature this has been linked to the reduction of Ni in $NiAl_2O_4$ and similar species in successive redox cycles.[25]

2.3. Redox regeneration

In a first step the regeneration with a redox treatment, i.e. the sequential exposure to CO_2 and H_2, was investigated. In Figure 8 the methane conversion over TOS and coke contents are shown for REF and all 1X1Ni samples. The results in Figure 7 show that for REF such a redox procedure reduces the deactivation in the second cycle. Such an effect can be seen for the Mn and the Cr series, especially with a high loading of promoter (see also Fig. S6). For the Fe series the conversion over TOS does not differ

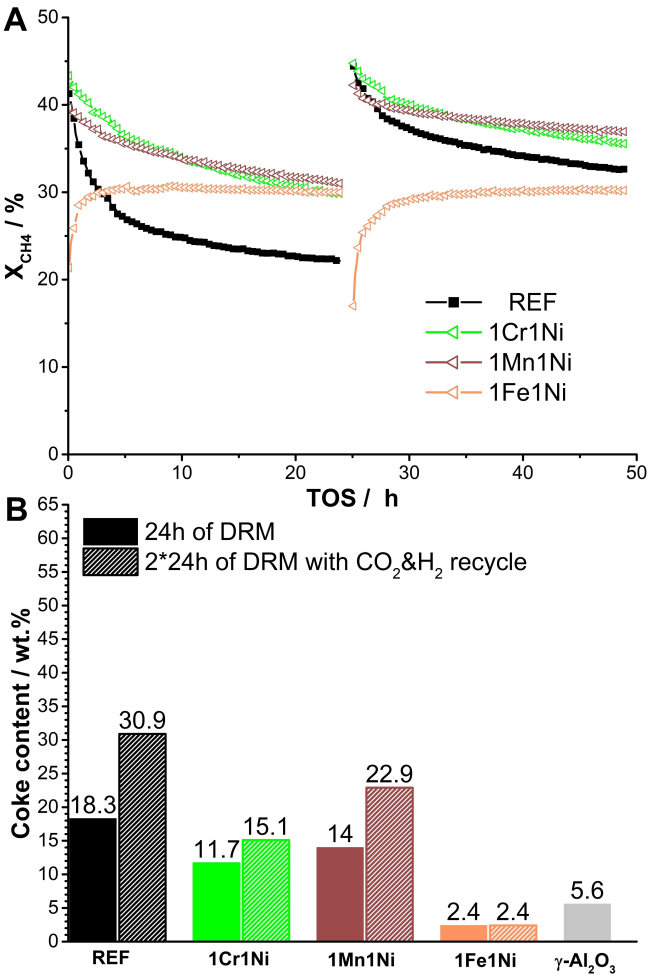

Figure 8. Methane conversion over TOS (A) and coke content after reaction (B – solid symbols 24 h of reaction, shaded symbols 2*24 h and regeneration) for the 1X1Ni samples before and after regeneration with CO_2 and H_2 (10 mg sample, 650 °C, 100 mL min^{-1} of 25 % CH_4, 25 % CO_2 in N_2).

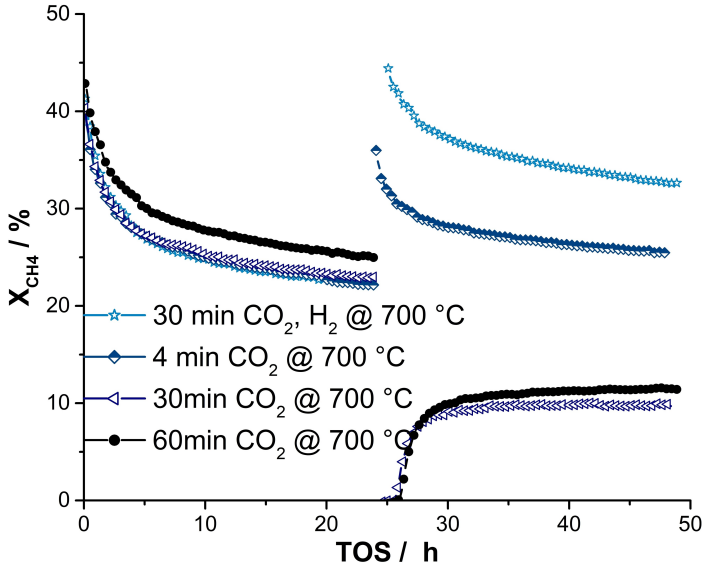

Figure 7. The effect of different regeneration protocols on pure Ni/Al_2O_3 (10 mg sample, 650 °C, 100 mL min^{-1} of 25 % CH_4, 25 % CO_2 in N_2).

much between the two cycles. Further differentiation is necessary when analyzing the coke content after reaction.

The reference Ni/Al_2O_3 undergoes a relative increase in coke content by almost 70% after one redox regeneration cycle to almost 31 wt.%. For the Mn and Cr-series the coke content of a redox-regenerated sample is comparable unless the promoter loading is high (Fig. S7). As can be seen in Figure 8, especially for 1Cr1Ni the increase in coking is contained. For the Fe-series the trend requires a more detailed explanation.

The results in Figure 9 reveal little difference in the conversion between the two dry reforming cycles for the Fe-containing catalysts. Only 0.25Fe1Ni deactivates slightly less after a redox regeneration. At the beginning of both reaction cycles 1Fe1Ni undergoes an induction period starting from almost the same level of conversion. After regeneration and another 24 h of DRM, the coke content of 1Fe1Ni is the same as after 24 h of dry reforming. For the samples with less iron, an increase in the coke content can be observed. 0.5Fe1Ni contains a similar coke amount as REF after two reaction periods and

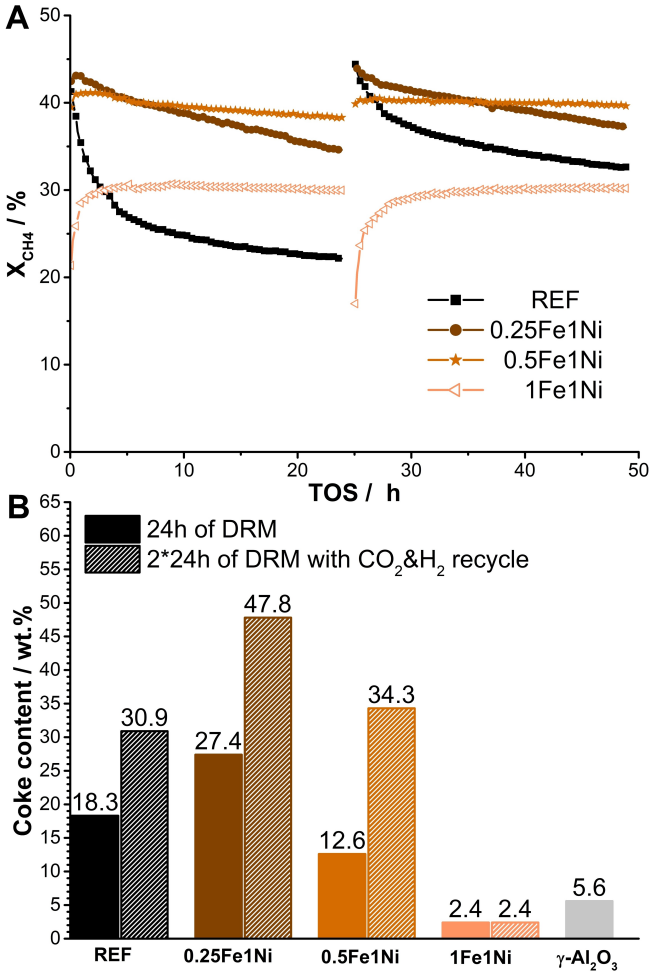

Figure 9. Conversion (A) and coke content (B – solid symbols 24 h of reaction, shaded symbols 2*24 h and regeneration) for two reaction periods and a redox regeneration procedure for the Fe-series of Ni/Al_2O_3 catalysts (10 mg sample, 650 °C, 100 mL min^{-1} of 25% CH_4, 25% CO_2 in N_2).

redox regeneration (34.3 wt.% vs 30.9 wt.%). However, for 0.25Fe1Ni the coke content increases to almost 50 wt.%.

As we highlighted in the introduction, more coke is formed on large Ni particles than small Ni particles (e.g. Ref. [8c]). In our previous work we investigated the effect of passivation and reactivation (i.e. a redox procedure) on Ni/Al_2O_3 systems used for dry reforming of methane.[25b] We determined that sintering during such treatments is common but it must be very pronounced to have an effect on the measurable catalytic conversion. The coke content on the other hand increases quickly, even when the catalyst sinters only moderately. We observed a similar increase in coking for the unpromoted sample REF as well as most promoted samples after redox regeneration. The combination of the H_2 chemisorption results and our previous detailed studies on this topic convinced us that the redox regeneration in this work leads to sintering of the catalyst and thus to the increase in coke formation. Additionally, the observed conversion profiles of REF, 0.25Mn1Ni and 0.25Cr1Ni are significantly more comparable after redox regeneration than for the fresh samples (Figure S6). All these findings indicate that such redox cycles strongly diminish the effect of Mn or Cr addition to Ni/Al_2O_3 except for high promoter loadings and highly effective promoters (e.g. the high stability of 1Cr1Ni).

The specifics of Fe–Ni interaction again require a separate interpretation of the data. To recall, Fe(0) dissolved in the Ni particles aides carbon diffusion and thus coke formation. FeO_x on the surface aides carbon oxidation. The increase in coke formation for 0.25Fe1Ni and 0.5Fe1Ni show that the Fe-series also sinter during redox regeneration. The complexity of the Fe–Ni system makes it impossible to judge based on the coke content if the degrees of sintering between the Fe series and REF are comparable. However, it can be clearly said, that sintering is not as pronounced as implied by H_2 chemisorption (Figure 3). Such strong sintering should influence the conversion profiles and the coke content of the sample 1Fe1Ni.

To sum up, both the chemisorption and reactivity data are strong indicators of sintering being the result of a redox regeneration. The sintering is so pronounced that a positive impact of the addition of Cr or Mn is mainly visible for high loadings. 1Mn1Ni still shows superior performance compared to REF but it is noticeably more affected than 1Cr1Ni. After redox regeneration it is also only for high Fe loadings that the coke content is still lower than for REF. For 0.5Fe1Ni and especially for 0.25Fe1Ni the coke content is higher than when using reference Ni/Al_2O_3.

2.4. Oxidative regeneration with CO_2

The results discussed in the previous section highlight the potential negative consequences of a redox regeneration. Furthermore, commercial applications of dry reforming are expected to involve ratios of CO_2/CH_4 larger than unity.[26] Especially in the upper section of a catalyst bed with little conversion the atmosphere can be oxidizing instead of reducing during methane reforming.[18] Therefore, it is of

interest to determine how resistant a catalyst is to oxidation and what the effect of the promoter is on this. For this the regeneration procedure of 4 minutes of diluted CO_2 at 700 °C is a good benchmark.

Figure 10 demonstrates the impact of such a regeneration procedure on the conversion and coke content for all 1X1Ni samples. The activity of reference Ni/Al_2O_3 after regeneration is slightly lower than for the first 24 h period. 1Cr1Ni is also only affected to a minimal degree, while for 1Mn1Ni the regeneration does not have any positive effect. 1Fe1Ni on the other hand is negatively affected by the CO_2 treatment and does not even reach 50% of the conversion before regeneration. The impact of the CO_2 treatment on the coke content differs between all samples. For REF, the coke content after the second reaction period is slightly lower than after the first. There is no visible impact for 1Cr1Ni but the coke content of 1Mn1Ni drops by 50% (14 vs 7.8 wt.%) after the short CO_2 exposure. For 1Fe1Ni the coke content actually increases.

The negative effect of the CO_2 treatment on catalyst stability increases noticeably, the higher the loading with Fe, as can be seen in Figure 11. However, only for 1Fe1Ni does the coke content increase after the CO_2 treatment. The other two samples form less coke after the CO_2 treatment.

We propose that the short exposure to CO_2 removes most of the coke and oxidizes some Ni without affecting the stabilizing effect of Cr. The increased CO_2 affinity of Mn means that at a higher Mn-loading the oxidation of Ni is accelerated, reducing the activity. Fe has the strongest interaction with CO_2 and thus even more Ni is oxidized, possibly by reactive oxygen in the oxidized Fe. A higher percentage of NiO means that less coke can be formed. This is in line with the lower coke content after oxidative regeneration observed for 0.25Fe1Ni and 0.5Fe1Ni. The increase in coke content for 1Fe1Ni is most likely due to the extensive degree of catalyst deactivation during the regeneration. Exposing the thus deactivated catalyst to the reaction mixture would then lead to the formation of coke species not in contact with catalytically active metal particles on the catalyst surface. These deposits are then not oxidized by iron species during dry reforming.

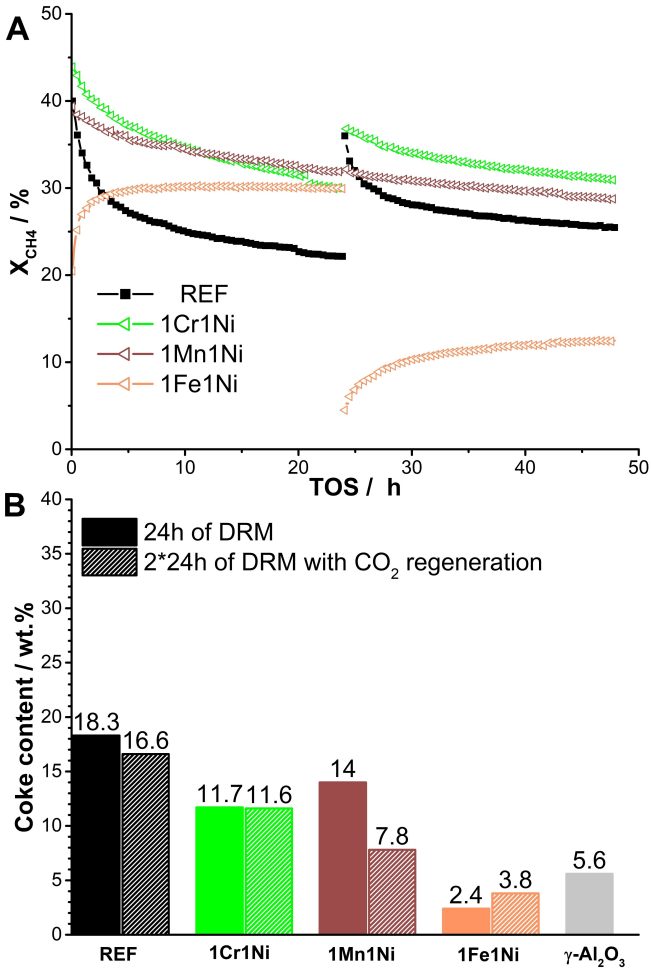

Figure 10. Conversion (A) and coke content (B – solid symbols 24 h of reaction, shaded symbols 2*24 h and regeneration) before and after regeneration with CO_2 for the samples 1X1Ni (10 mg sample, 650 °C, 100 mL min^{-1} of 25% CH_4, 25% CO_2 in N_2).

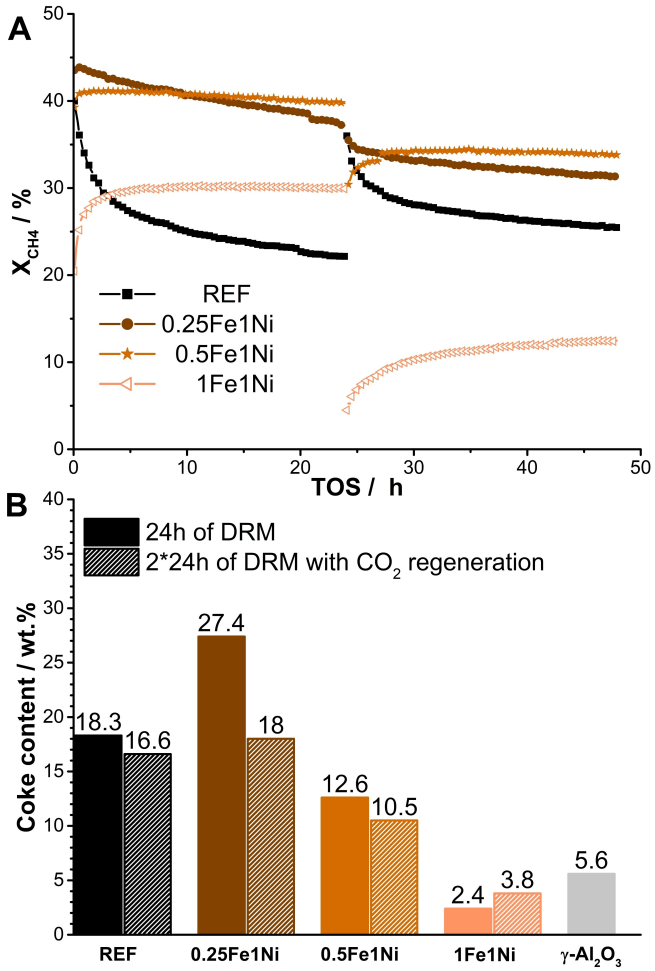

Figure 11. Conversion (A) and coke content (B – solid symbols 24 h of reaction, shaded symbols 2*24 h and regeneration) for two reaction periods and a CO_2 regeneration procedure for the Fe-series of Ni/Al_2O_3 catalysts (10 mg sample, 650 °C, 100 mL min^{-1} of 25% CH_4, 25% CO_2 in N_2).

Furthermore, we analyzed the coke content after 4 minutes of exposure to CO_2 at 700 °C without any additional dry reforming afterwards (Figure S10). In most cases the remaining coke amount on the catalyst is comparable to the carbon deposited on pure γ-Al_2O_3. The only noteworthy exceptions are 0.25Fe1Ni and 0.5Mn1Ni with higher coke contents. TEM analysis clearly shows that most carbon is present as carbon fibers (Figure S11), but other carbon species may be formed as well. Carbon fibers are oxidized at 700 °C but species such as low-surface area graphite require higher oxidation temperatures.[15b] This is a possible explanation but the impact of the promoters on the carbon structure is not within the scope of this work.

As discussed above, the choice of promoter has a strong impact on the rate of catalyst oxidation in the presence of CO_2. Therefore, we investigated the impact of an elevated CO_2 concentration on the catalyst stability. 50 mg of 1Fe1Ni were tested for 30 h in DRM with a CO_2/CH_4 ratio of 2. The elevated CO_2 concentration led to the detection of only 0.4 wt.% carbon after reaction. Figure 12 shows, that operation under such conditions leads to a distinct color change in the upper section of the catalyst bed. The reduced Ni catalysts studied in this work are always black, whereas the upper section of the catalyst bed is brown, i.e. the color of the freshly calcined sample. This is a clear sign of oxidation.

To further investigate the impact of CO_2 on this catalyst, freshly reduced 1Fe1Ni was treated with diluted (10% in He) CO_2 at 650 °C in another setup allowing for simultaneous operando monitoring of the catalyst bed and of the outlet gas composition with an IR detector. As shown in Figure 13, a color change over the catalyst bed could be observed over the course of the CO_2 treatment. The dark color typical of the reduced catalyst was progressively replaced by a visibly lighter tone. Monitoring the outlet gas composition via FTIR led to the detection of a CO signal over the entire experimental runtime of 50 minutes. At the very beginning of the measurement a peak in the CO signal of around 2 vol% was detected with a subsequent continuous drop of the measured concentration. After around 10 minutes TOS the CO concentration was in the range of 0.1 vol% and stayed in this order of magnitude. The combination of color change and CO detection in the outlet stream strongly supports the previous assumption of catalyst oxidation for the experiment with $CO_2/CH_4 = 2$.

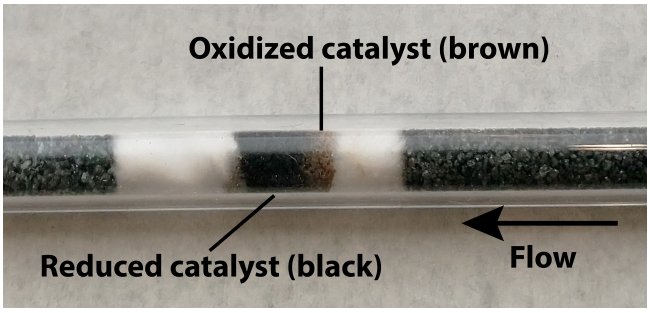

Figure 12. 1Fe1Ni after 30 h of reaction (50 mg sample, 650 °C, 100 mL min^{-1} of 12.5% CH_4, 25% CO_2 in N_2).

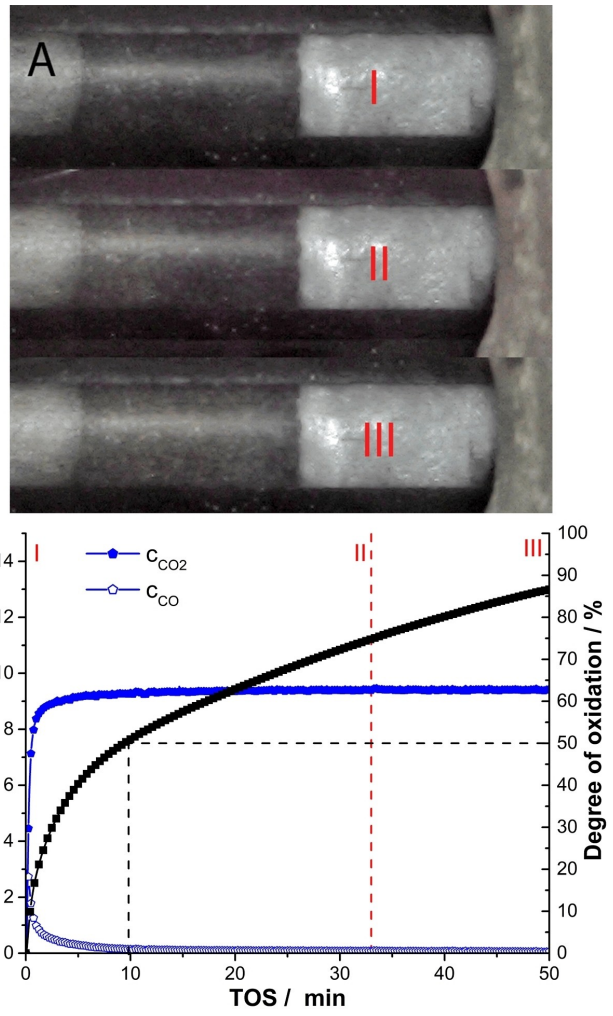

Figure 13. 1Fe1Ni during exposure to CO_2 at 650 °C (A – operando images, B – CO and CO_2 outlet concentrations and total degree of catalyst oxidation; 50 mg, 40 mL mi^{n-1} of 10% CO_2 in He).

The calculated degree of oxidation is also shown in Figure 13. The CO peak in the first 10 minutes TOS corresponds to an oxidation of 50% of the metal deposited on the catalyst surface. After 10 min TOS, the degree of oxidation increased at a lower and almost constant speed to approx. 86% at the end of the experiment. We attribute these two phases of oxidation to a fast oxidation of iron and a slow oxidation of Ni. Consequently, the CO peak represents a full oxidation of the Fe species of the catalyst in the initial phase of the CO_2 treatment.

The low CO concentration after 10 minutes TOS (0.1 vol% or less) means that the calculated degree of Ni oxidation may not be an exact value. A small difference between the calculated and the actual CO concentration over 40 minutes will quickly result in a non-negligible offset in the degree of oxidation as well. However, the data allow for two statements. The oxidation of Ni appears to be the decisive parameter for a color change of the catalyst. Additionally, a full oxidation of all Ni is not

necessary for a color change. After 50 minutes the rate of CO generation is still constant despite the color change being complete (Figure S15). These considerations also explain why after 33 min TOS (point II) only 30–40% of the catalyst had changed color when the CO quantification indicates a total degree of oxidation of 70-80%, i.e. 40–60% of Ni oxidation.

3. Conclusions

The impact of the CO_2 affinity of different promoters was tested on the stability of Ni/Al_2O_3 catalysts for dry reforming of methane. The focus of this comparison was to subject the catalysts to different regeneration procedures with CO_2 and H_2. Many academic studies use a CO_2/CH_4 ratio of unity. Under industrial conditions the feed will contain significantly greater oxidant (CO_2 or H_2O) concentrations. The differing regeneration procedures were implemented to simulate the impact of higher oxidant concentrations on a timescale sufficiently short for academic research. To back up the conclusions drawn from the activity tests the samples were also characterized with methods such as H_2 chemisorption, TPR and TEM. The promoters in question (Cr, Mn and Fe) were chosen to increase the CO_2 affinity step by step while keeping the promoter characteristics as similar as possible.

The combination of activity measurements and characterization clearly showed that regeneration of the catalysts via redox cycles leads to considerable sintering and thus an increase in coke formation. The sintering during regeneration also causes positive effects of promoter addition to disappear quickly unless a considerable amount of promoter is present on the samples. Additionally, the higher the CO_2 affinity of the promoter in question, the more quickly the respective catalysts appear to be oxidized by a treatment with CO_2. This research clearly emphasizes downsides of promoters such as Fe, that reduces the coke content via a Mars –van Krevelen mechanism. Consequently, if such promoters are desired in an industrial catalyst, the sintering resistance of the catalyst must be increased by other means, e.g. an improved support or improved synthesis methods such as via hydrotalcite-like precursors.[24]

Acknowledgements

Financial support by the CatC1Chem project of NWO, BASF, SABIC and Sasol is gratefully acknowledged. D.P. and A.U. thank JST PRESTO (grant no. JPMJPR16S3). E.A.U. acknowledges the partial support of the Tyumen region by a grant to non-profit organizations no. 89-don.

Conflict of Interest

The authors declare no conflict of interest.

Keywords: Heterogeneous catalysis · dry reforming of methane · catalyst regeneration · nickel · catalyst deactivation

[1] a) A. Ramirez, A. Dutta Chowdhury, A. Dokania, P. Cnudde, M. Caglayan, I. Yarulina, E. Abou-Hamad, L. Gevers, S. Ould-Chikh, K. De Wispelaere, V. van Speybroeck, J. Gascon, *ACS Catal.* **2019**, *9*, 6320–6334; b) J. Wei, Q. Ge, R. Yao, Z. Wen, C. Fang, L. Guo, H. Xu, J. Sun, *Nat. Commun.* **2017**, *8*, 15174.
[2] a) A. Bansode, A. Urakawa, *J. Catal.* **2014**, *309*, 66–70; b) E. Lam, K. Larmier, P. Wolf, S. Tada, O. V. Safonova, C. Copéret, *J. Am. Chem. Soc.* **2018**, *140*, 10530–10535; c) J. Zhong, X. Yang, Z. Wu, B. Liang, Y. Huang, T. Zhang, *Chem. Soc. Rev.* **2020**, *49*, 1385–1413.
[3] a) S. Arora, R. Prasad, *RCS Adv.* **2016**, *6*, 108668–108688; b) J. R. Rostrup-Nielsen, J. Sehested, J. K. Nørskov, in *Adv. Catal., Vol. 47*, Academic Press, **2002**, pp. 65–139; c) K. Wittich, M. Krämer, N. Bottke, S. A. Schunk, *ChemCatChem* **2020**, *12*, 2130–2147.
[4] IPCC, *Climate Change 2007: Synthesis Report. Contribution of Working Groups I, II and III to the Fourth Assessment Report of the Intergovernmental Panel on Climate Change*, Geneva, Switzerland, **2007**.
[5] T. Roussière, PhD thesis, Karlsruhe Institute of Technology (Karlsruhe), **2013**.
[6] Linde AG, Technologies that do more with less, https://www.linde-engineering.com/en/about-linde-engineering/success-stories/technologies-more-with-less.html, 2019 (accessed Nov. 19, 2019).
[7] Y. T. Shah, T. H. Gardner, *Catal. Rev.* **2014**, *56*, 476–536.
[8] a) H. S. Bengaard, J. K. Nørskov, J. Sehested, B. S. Clausen, L. P. Nielsen, A. M. Molenbroek, J. R. Rostrup-Nielsen, *J. Catal.* **2002**, *209*, 365–384; b) J. R. Rostrup-Nielsen, *J. Catal.* **1984**, *85*, 31–43; c) C. Vogt, J. Kranenborg, M. Monai, B. M. Weckhuysen, *ACS Catal.* **2020**, *10*, 1428–1438.
[9] a) H. S. Bengaard, I. Alstrup, I. Chorkendorff, S. Ullmann, J. R. Rostrup-Nielsen, J. K. Nørskov, *J. Catal.* **1999**, *187*, 238–244; b) R. Franz, T. Kuhlewind, G. Shterk, E. Abou-Hamad, A. Parastaev, E. Uslamin, E. J. M. Hensen, F. Kapteijn, J. Gascon, E. A. Pidko, *Catal. Sci. Technol.* **2020**, *10*, 3965–3974; c) J. Juan-Juan, M. C. Román-Martínez, M. J. Illán-Gómez, *Appl. Catal. A* **2006**, *301*, 9–15; d) T. Osaki, T. Mori, *J. Catal.* **2001**, *204*, 89–97.
[10] a) Z. Hou, O. Yokota, T. Tanaka, T. Yashima, *Appl. Surf. Sci.* **2004**, *233*, 58–68; b) S.-H. Seok, S. H. Choi, E. D. Park, S. H. Han, J. S. Lee, *J. Catal.* **2002**, *209*, 6–15; c) S.-H. Seok, S. H. Han, J. S. Lee, *Appl. Catal. A* **2001**, *215*, 31–38.
[11] M. Németh, D. Srankó, J. Károlyi, F. Somodi, Z. Schay, G. Sáfrán, I. Sajó, A. Horváth, *Catal. Sci. Technol.* **2017**, *7*, 5386–5401.
[12] a) Z. Hou, T. Yashima, *Catal. Lett.* **2003**, *89*, 193–197; b) D. Pakhare, J. Spivey, *Chem. Soc. Rev.* **2014**, *43*, 7813–7837; c) B. Pawelec, S. Damyanova, K. Arishtirova, J. L. G. Fierro, L. Petrov, *Appl. Catal. A* **2007**, *323*, 188–201; d) W. L. Vrijburg, G. Garbarino, W. Chen, A. Parastaev, A. Longo, E. A. Pidko, E. J. M. Hensen, *J. Catal.* **2020**, *382*, 358–371.
[13] a) M. Akri, S. Zhao, X. Li, K. Zang, A. F. Lee, M. A. Isaacs, W. Xi, Y. Gangarajula, J. Luo, Y. Ren, Y.-T. Cui, L. Li, Y. Su, X. Pan, W. Wen, Y. Pan, K. Wilson, L. Li, B. Qiao, H. Ishii, Y.-F. Liao, A. Wang, X. Wang, T. Zhang, *Nat. Commun.* **2019**, *10*, 5181; b) T. Roussière, K. M. Schelkle, S. Titlbach, G. Wasserschaff, A. Milanov, G. Cox, E. Schwab, O. Deutschmann, L. Schulz, A. Jentys, J. Lercher, S. A. Schunk, *ChemCatChem* **2014**, *6*, 1438–1446.
[14] a) A. More, S. Bhavsar, G. Veser, *Energy Technol-Ger* **2016**, *4*, 1147–1157; b) S. M. Kim, P. M. Abdala, T. Margossian, D. Hosseini, L. Foppa, A. Armutlulu, W. van Beek, A. Comas-Vives, C. Copéret, C. Müller, *J. Am. Chem. Soc.* **2017**, *139*, 1937–1949; c) S. A. Theofanidis, R. Batchu, V. V. Galvita, H. Poelman, G. B. Marin, *Appl. Catal. B* **2016**, *185*, 42–55; d) S. A. Theofanidis, V. V. Galvita, H. Poelman, G. B. Marin, *ACS Catal.* **2015**, *5*, 3028–3039.
[15] a) N. N. Nichio, C. E. Quincoces, M. G. González, P. Moral, in *Stud. Surf. Sci. Catal., Vol. 139* (Eds.: J. J. Spivey, G. W. Roberts, B. H. Davis), Elsevier, **2001**, pp. 263–269; b) H. Düdder, K. Kähler, B. Krause, K. Mette, S. Kühl, M. Behrens, V. Scherer, M. Muhler, *Catal. Sci. Technol.* **2014**, *4*, 3317–3328; c) M. Steib, Y. Lou, A. Jentys, J. A. Lercher, *ChemCatChem* **2017**, *9*, 3809–3813; d) S. Takenaka, E. Kato, Y. Tomikubo, K. Otsuka, *J. Catal.* **2003**, *219*, 176–185.
[16] A. Gil, A. Diaz, M. Montes, *J. Chem. Soc. Faraday Trans.* **1991**, *87*, 791–795.
[17] M. Steib, A. Jentys, J. A. Lercher, *J. Phys. Conf. Ser.* **2016**, *712*, 012049.

[18] A. Giehr, L. Maier, S. A. Schunk, O. Deutschmann, *ChemCatChem* **2018**, *10*, 751–757.
[19] A. J. van Dillen, R. J. A. M. Terörde, D. J. Lensveld, J. W. Geus, K. P. de Jong, *J. Catal.* **2003**, *216*, 257–264.
[20] M. G. González, N. N. Nichio, B. Moraweck, G. Martin, *Mater. Lett.* **2000**, *45*, 15–18.
[21] F. Kapteijn, A. D. Vanlangeveld, J. A. Moulijn, A. Andreini, M. A. Vuurman, A. M. Turek, J. M. Jehng, I. E. Wachs, *J. Catal.* **1994**, *150*, 94–104.
[22] W. L. Vrijburg, E. Moioli, W. Chen, M. Zhang, B. J. P. Terlingen, B. Zijlstra, I. A. W. Filot, A. Züttel, E. A. Pidko, E. J. M. Hensen, *ACS Catal.* **2019**, *9*, 7823–7839.
[23] a) K. Tomishige, D. Li, M. Tamura, Y. Nakagawa, *Catal. Sci. Technol.* **2017**, *7*, 3952–3979; b) G. Wang, Y. Jin, G. Liu, Y. Li, *Energy Fuels* **2013**, *27*, 4448–4456.
[24] D. Li, M. Koike, L. Wang, Y. Nakagawa, Y. Xu, K. Tomishige, *ChemSusChem* **2014**, *7*, 510–522.
[25] a) L. Silvester, D. Ipsakis, A. Antzara, E. Heracleous, A. A. Lemonidou, D. B. Bukur, *Energy Fuels* **2016**, *30*, 8597–8612; b) R. Franz, F. D. Tichelaar, E. A. Uslamin, E. A. Pidko, *Appl. Catal. A* **2021**, *612*, 117987.
[26] A. Ramirez, K. Lee, A. Harale, L. Gevers, S. Telalovic, B. Al Solami, J. Gascon, *ChemCatChem* **2020**, *12*, 5919–5925.

Manuscript received: July 16, 2021
Revised manuscript received: September 26, 2021
Accepted manuscript online: September 27, 2021
Version of record online: ■■, ■■■

FULL PAPERS

Heterogeneous catalysis: Ni/Al_2O_3 catalysts with different promoters were tested in dry reforming of methane and regenerated under different conditions. This allows for a detailed comparison of promoter effects under different regimes. Ni/Al_2O_3 with high Fe loadings operates stably for $CO_2/CH_4 = 1$ but quickly deactivates for higher CO_2 concentrations.